Acta Cryst. (1999). B**55**, 467–483

Cluster configurations in modulated $EuV_xMo_{8\pm y}O_{14}$ crystals

H. Leligny,[a]* D. Grebille,[a] P. Roussel,[a] Ph. Labbé,[a] M. Hervieu,[a] B. Raveau,[a] J. Tortelier[b] and P. Gougeon[b]

[a]*Laboratoire CRISMAT (UMR CNRS 6508), ISMRA, 14050 Caen CEDEX, France, and* [b]*Laboratoire de Chimie du Solide et Inorganique Moléculaire, UMR CNRS 6511, Université de Rennes 1, 35042 Rennes CEDEX, France. E-mail: h.leligny@crismat.ismra.fr*

(*Received 24 July 1998; accepted 8 January 1999*)

Abstract

Three orthorhombic crystals of chemical formula $Eu_xV_yMo_{8\pm z}O_{14}$ were investigated by X-ray diffraction (Mo $K\alpha$ radiation, $\lambda = 0.71073$ Å). They have nearly the same lattice parameters ($a \simeq 11.3$, $b \simeq 10.0$, $c \simeq 9.2$ Å), display one-dimensional incommensurate modulations of wavevector $\mathbf{q}^* = \gamma\mathbf{c}^*$ and are characterized by the same superspace group $Cmca(00\gamma)s00$. The crystals differ both in their compositions (namely $Eu_{0.976(6)}V_{1.13(5)}Mo_{7.10(5)}O_{14}$, $Eu_{0.986(4)}V_{1.10(3)}Mo_{7.30(1)}O_{14}$ and $EuMo_{7.96(1)}O_{14}$) and in their γ components [0.195 (2), 0.245 (2) and 0.286 (3), respectively]. The average structures of these crystals appear closely related to the structures of $LaMo_{7.7}O_{14}$ (not modulated) and $LaMo_8O_{14}$ (modulated); however, two main differences are outlined: first, the modulation direction is **c** in the Eu-containing crystals but **b** in the modulated La-containing crystal [$\mathbf{q}^* = (1/3)\mathbf{b}^*$], second, the Eu-containing crystals have centrosymmetric structures while the La-containing crystals have polar structures (space group $C2ca$). The Mo (or Mo and V) atoms are stacked to form (001) layers of metallic clusters. The density modulation of these structures implies the existence of the new types of clusters Mo_9, Mo_{10}, Mo_6V_4, Mo_7V_3 and Mo_8V_2 besides the clusters M_8 (Mo_8, Mo_6V_2 and Mo_7V) and M_7 (Mo_7 and Mo_6V) which are already known. Mo_8 units with *cis* and *trans* configurations and Mo_6V_2 units with a *trans* configuration appear as the main cluster types in these crystals. The nature of the metallic clusters changes along **c**, but inside one (001) layer it is likely that only one cluster type with a given configuration is present. The main structural result is the formation, in some unit cells, of strong intercluster Mo—Mo, Mo—V or V—V bonds with distances close to 2.6 Å within a layer as well as between two neighbouring layers.

1. Introduction

Since the report of the crystal structure of $Zn_2Mo_3O_8$ (McCarroll *et al.*, 1957), which contains triangular Mo_3 clusters, a large number of ternary and quaternary reduced molybdenum oxides exhibiting various types of metallic clusters has been synthesized and studied. Almost all of these clusters result from the association of octahedral Mo_6 clusters; for instance, in the $RE_{16}Mo_{21}O_{56}$ (RE = La, Ce, Pr, Nd) compounds (Gall & Gougeon, 1993) Mo_{10} clusters built from two edge-sharing Mo_6 octahedral units are observed.

More recently, evidence has been obtained for the new types of clusters Mo_7 and Mo_8, obtained by capping one or two faces of the Mo_6 octahedron. While the Mo_7 cluster has only been observed in coexistence with the tricluster Mo_7–Mo_{10}–Mo_7 in $Sr_4Ga_3Mo_{26}O_{48}$ (Tortelier & Gougeon, 1996), the Mo_8 cluster has been found alone in the polymorphic $REMo_8O_{14}$ (RE = La, Ce, Pr, Nd, Sm) compounds synthesized either by fused-salt electrolysis (La) or by high-temperature solid-state reaction (Ce, Pr, Nd, Sm). Four different crystal types were discovered in this last family. The RE–O network and the Mo_6 core of the bicapped Mo_8 clusters in all of these crystal types are similar, the only difference arising from the arrangement of the capped Mo atoms of the Mo_8 clusters. The first crystal type, found for $LaMo_{7.7}O_{14}$ (Leligny *et al.*, 1990), $NdMo_8O_{14}$ (Gougeon & McCarley, 1991) and $SmMo_8O_{14}$ (Tortelier & Gougeon, 1997), has an orthorhombic polar structure. The Mo_8 clusters in this crystal type are stacked to form layers and have a single configuration, the *cis* one. The second crystal type, which is characteristic of the stoichiometric $LaMo_8O_{14}$ compound (Leligny *et al.*, 1993), shows a similar orthorhombic polar structure, but a commensurate modulation with a wavevector $\mathbf{q}^* = \mathbf{b}^*/3$ parallel to the cluster layers is present; *cis* and *trans* configurations are observed for the Mo_8 clusters inside each metallic layer but the layer distribution of these clusters is governed by a probability law corresponding to the density modulation. The *cis* configuration is the predominant one (65%). More recently, we have obtained a third crystal type for $LaMo_8O_{14}$ (Kerihuel *et al.*, 1996) and $CeMo_8O_{14}$ (Kerihuel & Gougeon, 1995*a*) and a fourth one for $PrMo_8O_{14}$ (Kerihuel & Gougeon, 1995*b*) by high-temperature solid-state reaction; in these compounds the Mo networks are built from well ordered mixtures of Mo_8 clusters in *cis* and *trans* configurations, in equal proportion for the La and Ce compounds and in the ratio 2:1 for $PrMo_8O_{14}$.

ISSN 0108-7681

In all these crystals except the modulated La-containing crystals a perfect long-range order is observed for the cluster distribution within a particular layer as well as between adjacent layers. Other than this, it has been shown that the interactions between clusters are weak.

Although bond length–bond strength calculations clearly indicate that the number of electrons for the *cis* isomeric form of the Mo_8 cluster could vary from 22 in $LaMo_8O_{14}$ to 23 in $NdMo_8O_{14}$, attempts to synthesize isostructural compounds by substituting a divalent cation (Ca, Sr, Ba or Eu) for the trivalent rare earth were unsuccessful. However, a reaction with a nominal composition '$EuVMo_{10}O_{16}$' gave as its major product an interesting new compound. Its lattice is closely related to that of the modulated phase $LaMo_8O_{14}$ (they have the same cell parameters), but an incommensurate modulation with a wavevector along **c*** (**q*** = γ**c***), rather than along **b***, is seen.

We report here the study of the modulated structures of three $EuV_xMo_{8\pm y}O_{14}$ crystals with different compositions and different γ values, and we examine the action of the modulation on the distribution and the geometry of the different types of metallic clusters.

2. Experimental

2.1. *Crystal growth*

Starting reagents were Eu_2O_3 (Rhône–Poulenc, 99.999%), V_2O_5 (Merck, 99%), MoO_3 (Strem Chemicals, 99.9%) and Mo (Cimebocuze, 99.9%), all in powder form. The rare-earth oxide was pre-fired at 1273 K before use and the Mo powder was heated under a hydrogen flow at 1273 K for 6 h. The stoichiometric mixture was pressed into a *ca* 5 g pellet, loaded into a molybdenum crucible (depth 2.5 cm, diameter 1.5 cm, previously cleaned by heating at 1800 K for 15 min under a dynamic vacuum of about 10^{-5} Torr) and then sealed under a low pressure of argon using an arc-welding system. Single crystals were obtained by heating the charge at a rate of 300 K h^{-1} to *ca* 2220 K and keeping it at this temperature for 5 min. The charge was then cooled at a rate of 100 K h^{-1} to 1373 K and finally furnace-cooled. The crystals were generally obtained as black irregular fragments.

2.2. *X-ray diffraction*

The quality of the crystals was first checked and the crystal symmetry was established using both Weissenberg and precession photographs.

X-ray data collections for three different crystals were performed using graphite-monochromated Mo $K\alpha$ radiation (λ = 0.71073 Å) on an Enraf–Nonius CAD-4 diffractometer driven by a program which allowed the satellite reflections in incommensurate positions to be measured. The cell parameters were determined from standard techniques using 25 main reflections for each crystal with θ in the range 25–35°. To define the component q_3^* of the modulation wavevector of each crystal studied, some reciprocal rows [001]* (chosen by inspection of the precession photographs) were scanned. Corrections for Lorentz and polarization effects were applied to the data. Absorption corrections were applied with the program *JANA*98 (Petricek & Dusek, 1998) using an approximate model for the crystal morphology. Further details are given in Table 1.†

2.3. *Transmission electron microscopy and EDS analysis*

An electron microscopy study was performed on several samples prepared by crushing single crystals selected from the same batch; the small flakes were suspended in alcohol and then deposited on a holey carbon film. They were studied with a Jeol 200CX electron microscope fitted with a eucentric goniometer (tilt ± 60° and rotation ± 180°). The reciprocal space was reconstructed by tilting around the three crystallographic axes. EDS (energy-dispersive spectroscopy) analysis was also carried out on several microcrystals to determine the V:Mo molar ratio.

3. Preliminary study and crystal symmetry

X-ray and electron diffraction (ED) experiments led to the following results. The diffraction patterns of all the crystals studied show two reflection subsets consisting of strong spots drawing an orthorhombic lattice and weak spots in nearly commensurate positions, interpreted as main and satellite reflections, respectively; all the reflections conform to *mmm* Laue symmetry. Only satellite reflections of first order defined by the modulation wavevector **q*** = γ**c*** are observed by X-ray diffraction; in contrast, satellite reflections of first and second order are clearly visible in reciprocal space by electron diffraction. This is illustrated in Fig. 1(*a*), which shows a [1$\bar{1}$0] ED pattern for a crystal with $\gamma \simeq 1/5$.

It was discovered that the modulation period along **c** depends on the sample; indeed, different values relatively close to 1/6, 1/5, 1/4 and 2/7 are found for the γ component. The intermediate value, ~1/5, is the value more frequently observed by electron microscopy. The γ components of the three crystals chosen for data collection are close to the rational values 1/5, 1/4 and 2/7 (Table 1), which can be considered as commensurate approximants. However, as a systematic deviation from the ideal positions was observed for the satellite peaks during the scanning procedure, the modulation was considered to be incommensurate within each crystal.

† Supplementary data for this paper are available from the IUCr electronic archives (Reference: LC0010). Services for accessing these data are described at the back of the journal.

Table 1. *Experimental data for $EuV_xMo_{8\pm y}O_{14}$*

	Crystal 1	Crystal 2	Crystal 3
Chemical formula	$Eu_{0.976(6)}V_{1.13(5)}$-$Mo_{7.10(5)}O_{14}$	$Eu_{0.986(4)}V_{1.10(3)}$-$Mo_{7.30(1)}O_{14}$	$EuMo_{7.96(1)}O_{14}$
Crystal shape (model)	Faces $(1\bar{1}0)$ $(\bar{1}10)$ (110) $(\bar{1}\bar{1}0)$ (001) $(00\bar{1})$	Faces (111) $(\bar{1}\bar{1}\bar{1})$ $(\bar{1}1\bar{1})$ $(1\bar{1}1)$ $(0\bar{1}0)$ $(\bar{1}\bar{1}0)$ (110)	Faces (111) $(1\bar{1}1)$ $(11\bar{1})$ $(\bar{1}1\bar{1})$ $(\bar{1}\bar{1}1)$ $(1\bar{1}\bar{1})$
Crystal size (μm)	48 × 72 × 400	50 × 120 × 145	75 × 162 × 188
Cell parameters (Å; T = 294 K)	a = 11.306 (1) b = 10.025 (1) c = 9.254 (1)	a = 11.325 (1) b = 10.024 (1) c = 9.240 (1)	a = 11.315 (1) b = 10.035 (1) c = 9.265 (1)
Modulation wavevector q^*	0, 0, 0.195 (2)	0, 0, 0.245 (2)	0, 0, 0.286 (3)
Superspace group	$Cmca(00\gamma)s00$	$Cmca(00\gamma)s00$	$Cmca(00\gamma)s00$
D_x (g cm^{-3}), Z, V (Å^3)	7.02, 4, 1048.9	7.15, 4, 1048.9	7.20, 4, 1052.0
Scan mode	ω–(2/3)θ	ω–θ	ω–θ
θ_{max} (°), $(\sin\theta/\lambda)_{max}$	45, 0.995	45, 0.995	45, 0.995
Registered space	$0 \le h \le 22$, $-19 \le k \le 19$, $0 \le l \le 18$, $-1 \le m \le 1$	$0 \le h \le 22$, $-19 \le k \le 19$, $0 \le l \le 18$, $-1 \le m \le 1$	$0 \le h \le 22$, $-19 \le k \le 19$, $0 \le l \le 18$, $-1 \le m \le 1$
No. of measured reflections	13 556	13 556	13 556
No. of main reflections with $I \ge 3\sigma(I)$ used in the refinement	1619	1542	1619
No. of satellite reflections with $I \ge 3\sigma(I)$ used in the refinement	1092	881	1076
Absorption coefficient μ(Mo $K\alpha$) (cm^{-1})	148.5	151.6	149.1
Maximum and minimum transmission factors	0.26, 0.42	0.23, 0.49	0.21, 0.52
R_{int} before absorption correction	0.044	0.052	0.055
R_{int} after absorption correction	0.030	0.031	0.029
R, R_0, R_1† (%)	4.11, 3.27, 7.63	4.11, 3.55, 6.55	4.78, 4.16, 7.46
wR, wR_0, wR_1† (%)	4.81, 4.33, 9.94	4.49. 4.16. 8.22	5.53, 5.21, 9.89
No. of observations/No. of refined parameters	20.5	18.1	22.4
$\Delta\rho_{max}$ (e Å^{-3})	3.5	3.0	4.0
$\Delta\rho_{min}$ (e Å^{-3})	−3.6	−3.7	−4.4
Scale factors K_0, K_1	0.248, 0.146	0.231, 0.153	1.069, 0. 660
K_1/K_0	0.59	0.66	0.62

† $R = \sum_{hklm} ||F_o| - |F_c|| / \sum_{hklm} |F_o|$, $wR = [\sum_{hklm} w(|F_o| - |F_c|)^2 / \sum_{hklm} w|F_o|^2]^{1/2}$ with $w = 1/\sigma^2_{F_o}$. R is for all reflections, R_0 is for main reflections $hkl0$ and R_1 is for satellite reflections $hkl\pm1$.

The reflection conditions established by X-ray and electron diffraction on several samples are the following: $hklm$, $h + k = 2n$; $0klm$, $m = 2n$; $h0lm$, $l = 2n$ ($h = 2n$); $hk00$, $h = 2n$ ($k = 2n$) (m is the satellite order and $\mathbf{s}^* = h\mathbf{a}^* + k\mathbf{b}^* + l\mathbf{c}^* + m\mathbf{q}^*$ is the diffraction vector describing the whole reflection). These conditions are consistent with the superspace group $Cmca(00\gamma)s00$, which is then common to all the crystals of formula $EuV_xMo_{8\pm y}O_{14}$. Particular attention was paid to the condition $m = 2n$ for the $0klm$ reflections which implies the superglide mirror (m, s); in the X-ray and electron diffraction patterns no satellite reflections $0klm$ were detected even after a long exposure time (Fig. 1*b*).

The basic structure of these crystals appears to be closely related to the structure of the non-modulated crystal $LaMo_{7.7}O_{14}$ (Leligny *et al.*, 1990) and to the basic structure of the modulated crystal $LaMo_8O_{14}$ characterized by the modulation wavevector $\mathbf{q}^* = (1/3)\mathbf{b}^*$ (Leligny *et al.*, 1993). Indeed, the cell parameters for the three phases are rather similar and the extinction rules concerning the single reflection set ($LaMo_{7.7}O_{14}$) and the main reflections (Eu- and La-containing modulated phases) are identical. Nevertheless, two main differences between the Eu- and La-containing modulated phases can be outlined. First, considering the modulation scheme, the direction of $\mathbf{q}^*$ is $\mathbf{c}^*$ in the Eu-containing crystals while it is $\mathbf{b}^*$ in the La-containing crystals. Second, the Eu-containing crystals have centrosymmetric structures owing to the existence of the (m, s) mirror, while the La-containing crystals have polar structures of average symmetry $C2ca$.

For all the samples investigated by electron diffraction the modulation appears to be uniformly spread throughout the crystal.

Although these crystals are characterized by a modulated structure, planar disorder phenomena are also present; some main reflections with small θ for the three crystals studied are merged to form diffuse [001]* streaks of non-negligible intensity. However, it is verified that most of the main reflections are sharp and the satellite reflections are well resolved with an angular width similar to those of the main reflections.

A large variation in the V:Mo ratio from 0.05 to 0.22 (average value 0.12) is observed across the different samples: the limiting values observed for [V] and [Mo] are 0.4, 1.6 (average value 0.85) and 6.7, 9.1 (average value 7.4), respectively (an experimental error of about 5% is expected for the V and Mo atomic percentages).

No clear correlation between the modulation period of the crystal and its chemical composition can be established from these experimental results.

An EDS analysis was also carried out on the V-containing crystals 1 and 2 used for data collection (see Table 1). The V:Mo ratios per Eu atom obtained were $V_{0.91(5)}Mo_{7.4(4)}$ and $V_{1.04(5)}Mo_{7.8(4)}$, respectively.

4. A structural model for the modulated crystals

First, the average structure was refined using the *F* values of the main reflections in the space group *Cmca* using the program *JANA*98 (Petricek & Dusek, 1998). The atomic positions of $LaMo_{7.7}O_{14}$ (Leligny *et al.*, 1990) were taken as starting values, replacing La by Eu. During this preliminary work V, which is likely to occupy some of the Mo sites in the crystal, was not taken into account. To allow a comparison between this phase and the related La-containing phases to be made, it was decided to assign the same notation to the atoms occupying the same positions in $LaMo_{7.7}O_{14}$; for instance, the sequence Mo(1), Mo(2), Mo(3), Mo(4) in the La-containing crystal, where Mo(1) and Mo(2) are related by the pseudo mirror m_{yz}, becomes the sequence Mo(1), Mo(3), Mo(4) in the Eu-containing crystal (see Table 2). Refinement using anisotropic displacement parameters (ADPs; Trueblood *et al.*, 1996) for Eu and Mo atoms and isotropic displacement parameters for O atoms led to homogeneous reliability (*R*) factors for the three crystals in the range 0.04–0.05. Let us point out the main results of this preliminary study for the three crystals. The electron density of Eu in the Fourier maps is spread out along **a**. This effect is also apparent in the large values of the U^{11} ADPs and implies significant modulated displacements for Eu along [100]. The Mo atom on the Mo(4) site also shows noticeable displacements along **c** as shown by the abnormal U^{33} ADP values. Smaller displacements are found for the other atoms. The average occupation of the Mo(4) site by Mo (a possible substitution of V for Mo is expected) is at most 0.49, 0.46 and 0.49 for crystals 1, 2 and 3, respectively.

Note that, in the La- as well as in the Eu-containing crystals, for each filled La (or Eu) site ten Mo sites are available. In $LaMo_{7.7}O_{14}$ (space group *C*2*ca*), the Mo(4) site is not fully filled (occupation 0.85) and the site labelled Mo(5), which is pseudo-equivalent to the Mo(4) site through the *y*0*z* plane, is empty. In the modulated crystal $LaMo_8O_{14}$, the Mo(5) site may be filled in some unit cells; the average populations of the pseudo-equivalent sites Mo(4) and Mo(5) are found to be quite complementary and are 0.78 and 0.22, respectively. The Eu-containing crystals demonstrate a limiting case where the Mo(4) and Mo(5) sites are symmetry-related by the m_{yz} mirror and are approximately half occupied. As a result, in the average structure of the Eu-containing crystals an unrealistic distance of 2.37 Å occurs between two adjacent Mo(4) atoms. This anomaly should be removed by both the displacive and the density-modulation wave acting on the Mo(4) site.

The average structure of the Eu-containing crystals (Fig. 2) can be described as being derived from a hexagonal 'O_{16}' close packing of O atoms. In the 'O_{16}' lattice, O atoms are partly replaced by Eu and are partly vacant according to the formula $EuO_{14}\square_1$. Eu atoms and O-atom vacancies are distributed in an ordered way. About half of the octahedral interstices are then occupied by Mo atoms. As a result, metallic clusters with average Mo_8 composition are formed and stack in (001) layers. Taking into account the O-atom vacancies located at the centre of the Mo_6 octahedral units (Fig. 2) the Mo(1) and Mo(3) atoms then have an $O_5\square$ octahedral environment; the Mo(4) atom, on the other hand, has an O_6 octahedral environment.

As second-order satellite reflections were not observed during the X-ray data collection, a harmonic model for the modulation was considered first. The components of the displacement vector $\mathbf{U}^{\mu}$ of the μth atom and the occupancy probability P^{μ} of the site μ by

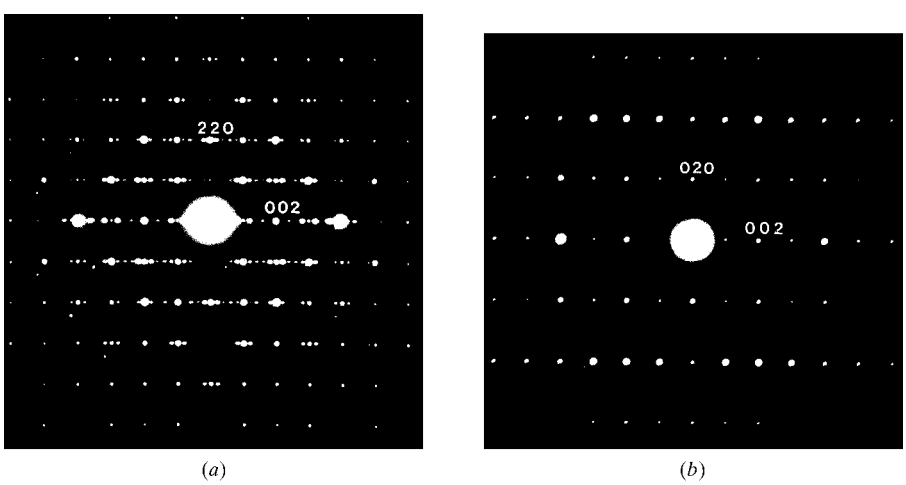

(*a*) (*b*)

Fig. 1. Electron diffraction patterns of $EuV_xMo_{8\pm y}O_{14}$. (*a*) The [1$\bar{1}$0] zone axis. Satellite reflections up to second order ($q_3^* \simeq 1/5$) are clearly visible. (*b*) The [100] zone axis. No 0*klm* satellites are observed.

Table 2. *Atomic parameters for the three crystals studied*

Uncertainties are given in parentheses. The average coordinates and the average occupancies are shown in the third column under the symbols $<r_0>$ and P_0. The A_1, B_1 and A_2, B_2 terms are the Fourier coefficients (of the cosine and sine terms) of the first and second harmonic, respectively, describing the displacive and density modulations. For Eu these are the standard harmonic coefficients of the displacement function. In the second part of the table for each crystal the ADP terms U^{ij} (Å^2) are given; the α_0^{ij} terms are the average values of the U^{ij} while the α^{ij} and β^{ij} terms are the Fourier coefficients (of the cosine and sine terms) of the ADP modulations which are assumed to be harmonic. B_{eq}(iso) for Eu and Mo, and B(iso) for O are also given. The ADP terms α_0^{ij} for V(4) (no modulation introduced) were constrained to be equal to those of Mo(4). $B_{eq} = 8\pi^2 U_{eq}$ with $U_{eq} = (1/3)\sum_{i=1}^{3}\sum_{j=1}^{3} U^{ij}a^{*i}a^{*j}\mathbf{a}_i\mathbf{a}_j$, reducing in the case of an orthorhombic crystal to $U_{eq} = (1/3)\sum_{i=1}^{3} U^{ii}$. The expression used for the Debye–Waller factor is $\exp(-2\pi^2 \sum_{i=1}^{3}\sum_{j=1}^{3} U^{ij}a^{*i}a^{*j}h_ih_j)$.

Crystal 1

		$<r_0>$, P_0	A_1	B_1	A_2	B_2
Eu	U_1	0.0022 (8)	0	0.040 (1)	0	0
	U_2	0	−0.004 (2)	0	0	0.005 (2)
	U_3	0	0.016 (1)	0	0	−0.019 (1)
	P	Δ = 0.488 (3)	$\bar{x}_{4,0} = 1/4$			
Mo(1)	U_1	−0.12075 (4)	0.0021 (2)	0.0040 (2)		
	U_2	0.07793 (4)	0.0016 (2)	−0.0062 (2)		
	U_3	0.37758 (4)	−0.0006 (2)	0.0021 (2)		
	P	0.93 (1)†				
Mo(3)	U_1	0	−0.0003 (2)	0.0036 (2)		
	U_2	−0.16077 (4)	0	0		
	U_3	0.38118 (5)	0	0		
	P	0.93 (1)†				
Mo(4)	U_1	0.2331 (8)	−0.0026 (6)	0.008 (1)		
	U_2	−0.1609 (8)	0.0025 (6)	−0.003 (1)		
	U_3	0.371 (1)	$U_{3,0}$ = −0.042 (1)	$\bar{x}_{4,0}$ = 0.33 (2)	$\Delta' = 1$	
	P	0.380 (4)	0.032 (8)	0.480 (8)	−0.14 (2)	−0.11 (1)
V(4)	U_1	0.2410 (6)	0.013 (1)	−0.006 (1)		
	U_2	−0.1656 (5)	−0.011 (1)	0.001 (2)		
	U_3	0.3783 (7)	$U_{3,0}$ = −0.028 (1)	$\bar{x}_{4,0}$ = 0.25 (2)	$\Delta' = 1$	
	P	0.178 (2)				
O(1)	U_1	0.2547 (5)	0	0.013 (1)		
	U_2	0	0.006 (1)	0		
	U_3	1/2	0.009 (1)	0		
O(2)	U_1	0	−0.003 (1)	0.001 (1)		
	U_2	−0.1596 (4)	0	0		
	U_3	−0.2388 (4)	0	0		
O(3)	U_1	−0.1227 (3)	0.000 (1)	−0.003 (1)		
	U_2	−0.0823 (3)	0.001 (1)	−0.002 (1)		
	U_3	0.2444 (4)	0.002 (1)	0.010 (1)		
O(5)	U_1	−1/4	0	−0.005 (1)		
	U_2	0.1694 (4)	0.003 (2)	0		
	U_3	1/4	0	0.013 (1)		
O(6)	U_1	0.1223 (3)	0.003 (1)	−0.003 (1)		
	U_2	0.2516 (3)	−0.002 (1)	0.008 (1)		
	U_3	0.4915 (4)	0.001 (1)	−0.003 (1)		

		α_0^{ij}	α^{ij}	β^{ij}	B_{eq} (Å^2)
Eu	U^{11}	0.023 (1)	0	0	1.58 (6)
	U^{22}	0.029 (2)	0	−0.022 (2)	
	U^{33}	0.0097 (5)	0	0	
	U^{12}	0	−0.012 (2)	0	
	U^{13}	0	0.032 (1)	0	
	U^{23}	−0.009 (1)	0	0.010 (2)	

Table 2 (*cont.*)

		α_0^{ij}	α^{ij}	β^{ij}	B_{eq} (Å^2)
Mo(1)	U^{11}	0.0043 (1)	0.0007 (6)	0.0005 (4)	0.426 (5)
	U^{22}	0.0060 (1)	−0.0008 (5)	−0.0016 (3)	
	U^{33}	0.0059 (1)	−0.0005 (5)	0.0007 (4)	
	U^{12}	0.0007 (1)	0.0013 (4)	0.0006 (3)	
	U^{13}	−0.0005 (1)	−0.0004 (3)	−0.0007 (3)	
	U^{23}	0.0015 (1)	−0.0011 (3)	−0.0007 (3)	
Mo(3)	U^{11}	0.0088 (2)	0	0	0.497 (8)
	U^{22}	0.0046 (2)	0	0	
	U^{33}	0.0055 (2)	0	0	
	U^{12}	0	0.0012 (6)	−0.0015 (5)	
	U^{13}	0	0.0005 (5)	−0.0012 (5)	
	U^{23}	0.0004 (1)	0	0	
Mo(4)	U^{11}	0.010 (2)	−0.016 (2)	0.000 (2)	0.84 (8)
	U^{22}	0.011 (2)	−0.007 (1)	−0.007 (2)	
	U^{33}	0.010 (2)	−0.007 (1)	−0.003 (2)	
	U^{12}	−0.004 (1)	0.010 (1)	0.000 (2)	
	U^{13}	−0.008 (1)	0.016 (1)	0.005 (2)	
	U^{23}	0.008 (1)	−0.009 (1)	−0.008 (2)	
O(1)	U	0.0100 (10)			0.79 (8)
O(2)	U	0.0082 (6)			0.65 (5)
O(3)	U	0.0100 (5)			0.79 (4)
O(5)	U	0.0077 (7)			0.61 (5)
O(6)	U	0.0112 (5)			0.88 (4)

Crystal 2

		$<r_0>$, P_0	A_1	B_1	A_2	B_2
Eu	U_1	0.0021 (6)	0	0.043 (1)	0	0
	U_2	0	−0.010 (2)	0	0	0.012 (2)
	U_3	0	0.014 (1)	0	0	−0.017 (1)
	P	Δ = 0.493 (2)	$\bar{x}_{4,0} = 1/4$			
Mo(1)	U_1	−0.12057 (4)	0.0021 (1)	0.0039 (1)		
	U_2	0.07766 (4)	0.0021 (1)	−0.0053 (1)		
	U_3	0.37728 (4)	−0.0008 (1)	0.0014 (2)		
Mo(3)	U_1	0	0.0004 (2)	0.0019 (2)		
	U_2	−0.16060 (5)	0	0		
	U_3	0.38162 (5)	0	0		
Mo(4)	U_1	0.238 (1)	−0.0090 (5)	0.001 (1)		
	U_2	−0.159 (1)	0.0033 (5)	−0.005 (1)		
	U_3	0.371 (3)	$U_{3,0}$ = −0.047 (1)	$\bar{x}_{4,0}$ = 0.31 (3)	Δ' = 1	
	P	0.325 (3)	0.026 (7)	0.45 (6)	−0.16 (1)	−0.04 (1)
V(4)	U_1	0.2424 (5)	0.0073 (8)	0.004 (2)		
	U_2	−0.1676 (4)	−0.0021 (8)	−0.004 (2)		
	U_3	0.377 (3)	$U_{3,0}$ = −0.027 (8)	$\bar{x}_{4,0}$ = 0.25 (3)	Δ' = 1	
	P	0.274 (6)	0.02 (1)	−0.06 (1)	0.12 (2)	−0.03 (3)
O(1)	U_1	0.2531 (4)	0	0.012 (1)		
	U_2	0	0.007 (1)	0		
	U_3	1/2	0.010 (1)	0		
O(2)	U_1	0	−0.002 (1)	−0.002 (1)		
	U_2	−0.1589 (4)	0	0		
	U_3	−0.2385 (5)	0	0		
O(3)	U_1	−0.1224 (3)	0.001 (1)	−0.003 (1)		
	U_2	−0.0835 (3)	0.002 (1)	−0.002 (1)		
	U_3	0.2449 (4)	0.001 (1)	0.007 (1)		

Table 2 (*cont.*)

		$<r_0>$, P_0	A_1	B_1	A_2	B_2
O(5)	U_1	−1/4	0	−0.004 (1)		
	U_2	0.1684 (5)	0.004 (2)	0		
	U_3	1/4	0	0.011 (1)		
O(6)	U_1	0.1221 (3)	0.003 (1)	−0.002 (1)		
	U_2	0.2508 (3)	−0.002 (1)	0.009 (1)		
	U_3	0.4910 (4)	0.001 (1)	0.000 (1)		

		α_0^{ij}	α^{ij}	β^{ij}	B_{eq} (Å^2)
Eu	U^{11}	0.020 (1)	0	0	1.42 (6)
	U^{22}	0.024 (2)	0	−0.016 (2)	
	U^{33}	0.0087 (5)	0	0	
	U^{12}	0	−0.018 (2)	0	
	U^{13}	0	0.033 (1)	0	
	U^{23}	−0.006 (1)	0	0.007 (2)	
Mo(1)	U^{11}	0.0047 (1)	0.0003 (6)	0.0003 (4)	0.403 (5)
	U^{22}	0.0068 (1)	−0.0017 (5)	−0.0016 (3)	
	U^{33}	0.0039 (1)	0.0002 (5)	−0.0002 (4)	
	U^{12}	0.0004 (1)	0.0009 (4)	0.0001 (3)	
	U^{13}	−0.0003 (1)	0.0008 (3)	−0.0010 (3)	
	U^{23}	0.0013 (1)	−0.0011 (3)	−0.0005 (3)	
Mo(3)	U^{11}	0.0092 (2)	0	0	0.474 (6)
	U^{22}	0.0051 (2)	0	0	
	U^{33}	0.0038 (2)	0	0	
	U^{12}	0	0.0009 (6)	−0.0020 (5)	
	U^{13}	0	0.0008 (5)	−0.0013 (5)	
	U^{23}	0.0006 (1)	0	0	
Mo(4)	U^{11}	0.023 (2)	−0.020 (1)	−0.016 (3)	1.3 (2)
	U^{22}	0.017 (2)	−0.012 (1)	−0.014 (2)	
	U^{33}	0.009 (1)	−0.009 (1)	0.001 (2)	
	U^{12}	−0.008 (1)	0.012 (1)	0.004 (2)	
	U^{13}	−0.011 (1)	0.019 (1)	0.007 (2)	
	U^{23}	0.004 (1)	−0.011 (1)	0.001 (2)	
O(1)	U	0.0080 (10)			0.63 (8)
O(2)	U	0.0070 (6)			0.55 (5)
O(3)	U	0.0094 (5)			0.74 (4)
O(5)	U	0.0071 (8)			0.56 (6)
O(6)	U	0.0090 (5)			0.71 (4)

Crystal 3

		$<r_0>$, P_0	A_1	B_1	A_2	B_2
Eu	U_1	0.006 (3)	0	0.0411 (5)	0	0
	U_2	0	−0.0110 (8)	0	0	0.013 (1)
	U_3	0	0.0152 (4)	0	0	−0.0180 (5)
	P	Δ = 0.500 (2)	$\bar{x}_{4,0} = 1/4$			
Mo(1)	U_1	−0.12065 (2)	0.0026 (1)	0.0035 (1)		
	U_2	0.07781 (2)	0.0016 (1)	−0.0056 (1)		
	U_3	0.37760 (2)	−0.0005 (1)	0.0020 (1)		
Mo(3)	U_1	0	−0.0002 (1)	0.0032 (1)		
	U_2	−0.16072 (2)	0	0		
	U_3	0.38119 (3)	0	0		
Mo(4)	U_1	0.2378 (2)	−0.0027 (2)	0.0008 (3)		
	U_2	−0.1623 (2)	0.0012 (2)	−0.0013 (3)		
	U_3	0.3726 (7)	$U_{3,0}$ = −0.0363 (3)	$\bar{x}_{4,0}$ = 0.33 (1)	Δ' = 1	
	P	0.489 (2)	0.027 (5)	0.448 (4)	0.00 (2)	−0.11 (1)

Table 2 (*cont.*)

		$<r_0>$, P_0	A_1	B_1	A_2	B_2
O(1)	U_1	0.2544 (3)	0	0.0144 (4)		
	U_2	0	0.0083 (7)	0		
	U_3	1/2	0.0101 (7)	0		
O(2)	U_1	0	−0.0027 (7)	−0.0026 (6)		
	U_2	−0.1588 (2)	0	0		
	U_3	−0.2390 (2)	0	0		
O(3)	U_1	−0.1223 (2)	0.0014 (6)	−0.0037 (4)		
	U_2	−0.0828 (2)	0.0021 (6)	−0.0020 (5)		
	U_3	0.2444 (2)	0.0068 (6)	0.0067 (6)		
O(5)	U_1	−1/4	0	−0.0062 (5)		
	U_2	0.1692 (2)	0.0048 (8)	0		
	U_3	1/4	0	0.0116 (6)		
O(6)	U_1	0.1219 (2)	0.0046 (6)	−0.0019 (4)		
	U_2	0.2516 (2)	−0.0032 (7)	0.0098 (4)		
	U_3	0.4914 (2)	0.0023 (6)	−0.0023 (6)		

		α_0^{ij}	α^{ij}	β^{ij}	B_{eq} (Å^2)
Eu	U^{11}	0.0176 (6)	0	0	1.10 (4)
	U^{22}	0.0154 (8)	0	−0.0057 (11)	
	U^{33}	0.0089 (2)	0	0	
	U^{12}	0	−0.0168 (8)	0	
	U^{13}	0	0.0296 (5)	0	
	U^{23}	−0.0034 (5)	0	0.0045 (7)	
Mo(1)	U^{11}	0.0033 (1)	0.0004 (3)	0.0006 (4)	0.355 (5)
	U^{22}	0.0067 (1)	−0.0016 (2)	−0.0018 (2)	
	U^{33}	0.0036 (1)	−0.0003 (3)	0.0005 (2)	
	U^{12}	0.0004 (1)	0.0005 (2)	−0.0002 (1)	
	U^{13}	−0.0004 (1)	0.0003 (2)	−0.0005 (2)	
	U^{23}	0.0013 (1)	−0.0010 (2)	−0.0004 (2)	
Mo(3)	U^{11}	0.0081 (1)	0	0	0.489 (5)
	U^{22}	0.0043 (1)	0	0	
	U^{33}	0.0032 (1)	0	0	
	U^{12}	0	0.0005 (3)	−0.0013 (2)	
	U^{13}	0	0.0012 (2)	−0.0014 (3)	
	U^{23}	0.0002 (1)	0	0	
Mo(4)	U^{11}	0.0173 (7)	−0.0119 (6)	−0.0093 (11)	0.94 (2)
	U^{22}	0.0080 (5)	−0.0040 (5)	−0.0015 (9)	
	U^{33}	0.0105 (5)	−0.0055 (4)	0.0016 (8)	
	U^{12}	0.0049 (1)	0.0054 (4)	0.0000 (8)	
	U^{13}	−0.0095 (6)	0.0119 (4)	0.0074 (9)	
	U^{23}	0.0041 (5)	−0.0058 (3)	−0.0032 (8)	
O(1)	U	0.0084 (5)			0.66 (4)
O(2)	U	0.0062 (3)			0.49 (2)
O(3)	U	0.0092 (2)			0.73 (2)
O(5)	U	0.0062 (4)			0.49 (3)
O(6)	U	0.0095 (3)			0.75 (2)

† $P_V = 1 - P_{Mo}$.

the μth atom were then written as a Fourier series limited to the first harmonic

$$U_i^\mu(\bar{x}_4^\mu) = A_i^\mu \cos 2\pi\bar{x}_4^\mu + B_i^\mu \sin 2\pi\bar{x}_4^\mu$$

(i = 1, 2, 3) and

$$P^\mu(\bar{x}_4^\mu) = P_0^\mu + C^\mu \cos 2\pi\bar{x}_4^\mu + D^\mu \sin 2\pi\bar{x}_4^\mu,$$

where P_o^μ is the average occupation and $\bar{x}_4^\mu = \mathbf{q}^*.(\mathbf{r}_0^\mu + \mathbf{p}) = \mathbf{q}^*.\mathbf{r}_0^\mu + t$ is an internal parameter; $\mathbf{r}_0^\mu$ denotes the average position of the μth atom in the

origin unit cell and **p** denotes a lattice vector. For an incommensurate modulation all the values of t in the 0, 1 interval are physical points (de Wolff *et al.*, 1981).

As no full order is likely to be established in the crystals, separate scale factors were introduced for the main reflections and the satellite reflections, the intensities of which are expected to be weakened. A first model of displacive modulation (harmonic), considering only the Eu atom and the Mo atom on the Mo(4) site, was obtained from trials including satellite reflections in the data set. Four-dimensional Fourier maps showed that the modulation model could be improved by using both an occupancy crenel function and a harmonic displacement function for Eu (Fig. 3), and introducing a sawtooth-like function for Mo on the Mo(4) site to take into account its rectilinear displacement along z (Fig. 4). An orthogonalization procedure (Petříček *et al.*, 1995; Boucher *et al.*, 1996) was used to derive the Eu displacive modulation.

The evolution with $\bar{x}_4$ of the occupation probability P of Eu is (Fig. 3) $P(\bar{x}_4) = 1$ for $\bar{x}_4 \in [\bar{x}_{4,0} - \Delta/2, x_{4,0} + \Delta/2] \bmod 1$. $P(\bar{x}_4) = 0$ outside this $\bar{x}_4$ range, where $\bar{x}_{4,0}$ is the midpoint of the non-zero interval ($\bar{x}_{4,0} \simeq 1/4$) and Δ is the width of this interval ($\Delta = 1/2$).

Note that the two Eu atoms symmetry-related by the superglide mirror (m, s) have complementary occupation functions.

The rectilinear displacement U_3 as a function of $\bar{x}_4$ for Mo on the Mo(4) site is given by $U_3 = 2U_{3,0}(\bar{x}_4 - \bar{x}_{4,0})/\Delta'$, where $U_{3,0}$ is the maximum amplitude displacement along z, $\bar{x}_{4,0}$ is the midpoint corresponding to zero displacement and Δ' is the $\bar{x}_4$ interval for the displacements.

Looking at the x_3, x_4 section Fourier map related to the Mo(4) site (Fig. 4), it appears that Δ' significantly exceeds the value of 0.5 which corresponds roughly to the limiting average occupation of Mo on the Mo(4) site. To account for this electron-density spread, the Δ' value was artificially fixed to one, but a density modulation $P(\bar{x}_4)$ modelled with two harmonics was introduced for Mo. Another model was also tried in which the Δ' parameter was allowed to vary and the previous density modulation was removed, but this led to higher R factors and abnormal values ($U^{22} < 0$) for the ADP terms. Particular care was taken to specify the substitution of V for Mo on the Mo sites. As no vacancy is expected on the Mo(1) and Mo(3) sites, it is easy to check if substitution of V for Mo is involved using the constraint $P_V + P_{Mo} = 1$. In contrast, no restraint can be applied *a priori* between P_V and P_{Mo} on the Mo(4) site. However, owing to the modulated occupation $P(\bar{x}_4)$ of Mo on the Mo(4) site and the noticeable difference between the anom-

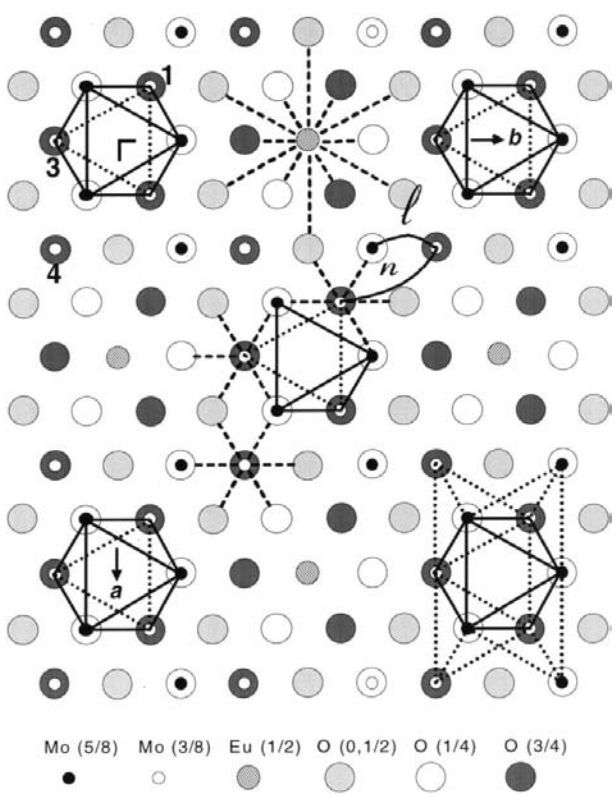

Fig. 2. A [001] projection of the average structure. This projection is drawn assuming a perfect hexagonal close packing for the O atoms (idealized structure) and only one (001) metallic layer (at z centred at 1/2) is shown. The adjacent (001) metallic layer (at $z = 0$) is obtained from this layer by a shift of **a**/2 (or **b**/2). The octahedral Mo_6 units are outlined and the three independent Mo atoms are shown by numbers. The expected metallic bonds between the Mo_6 unit and Mo (or V) likely to occupy the Mo(4) sites surrounding this metal octahedron are drawn with dotted lines. The Eu—O and Mo—O bonds are also indicated (dashed lines). The symbols l and n denote the possible interactions between the clusters within a particular layer.

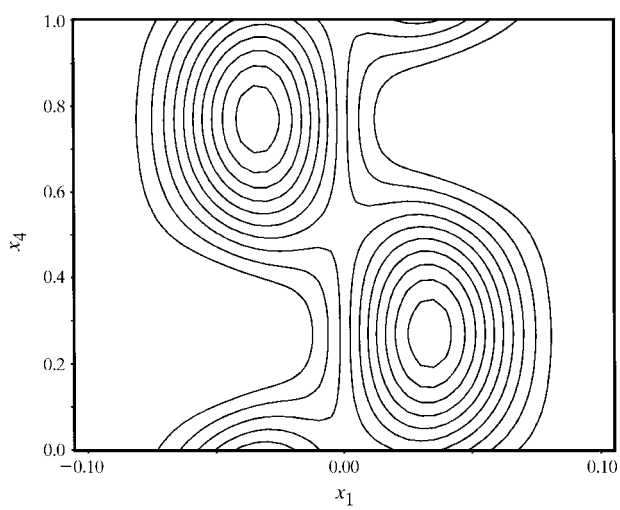

Fig. 3. x_1, x_4 section ($x_2 = 0, x_3 = 0$) of the four-dimensional Fourier map (F_{obs}) around the Eu atom. The electron density can be explained by a crenel-type density modulation.

alous-dispersion terms of V and Mo, a refinement of the amount of V on the Mo(4) site, and of its density modulation only in crystal 2, proved to be possible and resulted in smooth convergence.

To give sufficient weight to the satellite reflections (which are weak as a whole) a unitary weighting scheme was chosen rather than the classic scheme based on counting statistics. Finally, in order to detect any possible anomaly, a harmonic modulation of the ADP terms was considered for the Eu and Mo atoms. This noticeably improved the reliability factor R_1 of the satellite reflections. The final reliability factors on F, R (global), R_0 (main reflections), R_1 (satellite reflections) and the corresponding wR factors, are given in Table 1, while the refinement results for the three crystals studied are compared in Table 2. In the final difference Fourier maps some residual peaks with density less than 4 e $Å^{-3}$ were found around the Eu and Mo atoms at distances less than 1 Å.

5. Discussion

5.1. *The V:Mo ratios and chemical formulae*

The substitution of V for Mo at the Mo sites appears to be different in each of the three crystals studied. In the first crystal, characterized by $\gamma = 0.195\,(2)$, V partially occupies all of the Mo sites (see Table 2) but the refinement does not show any significant modulation of the V distribution. In the second crystal, characterized by $\gamma = 0.245\,(2)$, only the Mo(4) site is partially occupied by V and a significant occupation modulation is observed for this site (Table 2). In the third crystal, characterized by $\gamma = 0.286\,(3)$, it is curious that the presence of V is not confirmed by the refinement; nevertheless the presence of traces of V cannot be entirely excluded.

The density modulation of Mo on the Mo(4) site is established to be very significant for the three crystals. This density distribution is quite similar in the two crystals containing V but appears significantly more spread out in the third crystal. As an example, the Mo occupancy and the correlated V occupancy for the second crystal are shown *versus* t in Fig. 5 compared with the Mo occupancy variation of the third crystal. While Mo is distributed in only one type of zone in t centred on 0.15 in the second crystal, V preferentially occupies two types of zones in t centred on 0.40 and 0.85; note that in the crystal zone corresponding to $t \simeq 0.6$ the Mo(4) sites may be filled only by V atoms. The chemical formula deduced from the refinement results is given in Table 1 for each crystal studied.

5.2. *Evolution of the metal–oxygen bonds in the crystals*

Since the variations of the Eu—O and Mo—O distances as a function of t are relatively similar in the three crystals, this discussion is limited to the second crystal.

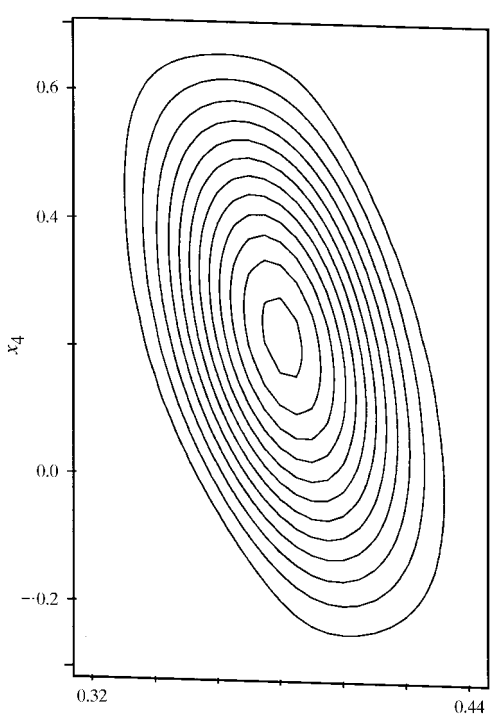

Fig. 4. x_3, x_4 section ($x_1 = 0.24$, $x_2 = -0.16$) of the four-dimensional Fourier map (F_{obs}) showing the rectilinear displacement $U_3(x_4)$ of Mo(4).

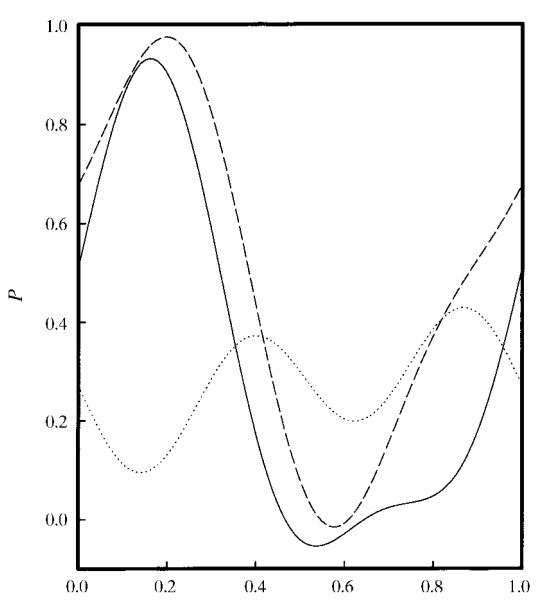

Fig. 5. The density modulation $P(t)$ at the Mo(4) site. The variation of P with t for Mo in crystal 2 (solid line) and in crystal 3 (dashed line) is compared. The density curve of V in crystal 2 is also shown (dotted line).

Table 3. *Mo—O and V—O distances (Å) in crystal 2*

	d_{min}	d_{max}	
Mo(1)—O(1^{xi})	1.943	2.130	$\sigma \simeq 0.004$ Å
Mo(1)—O(2^{iii})	2.032	2.056	
Mo(1)—O(3)	1.970	2.085	
Mo(1)—O(5)	2.037	2.145	
Mo(1)—O(6^{iv})	1.990	2.072	
Mo(3)—O(2^{xiii})	2.122	2.122	
Mo(3)—O(3)	2.016	2.040	
Mo(3)—O(3^{iv})	2.016	2.040	
Mo(3)—O(6^{x})	2.023	2.034	
Mo(3)—O(6^{xi})	2.023	2.034	
Mo(4)—O(1)†	1.95	2.00	$\sigma \simeq 0.05$ Å
Mo(4)—O(3^{iv})†	1.95	2.05	
Mo(4)—O(3^{xv})†	1.94	2.24	
Mo(4)—O(5^{xvi})†	1.95	2.23	
Mo(4)—O(6^{x})†	1.90	2.15	
Mo(4)—O(6^{xvii})†	2.08	2.13	
V(4)—O(1)	1.88	2.16	$\sigma \simeq 0.03$ Å
V(4)—O(3^{iv})	1.75	2.16	
V(4)—O(3^{xv})	1.98	2.24	
V(4)—O(5^{xvi})	1.92	2.29	
V(4)—O (6^{x})	1.80	2.12	
V(4)—O(6^{xvii})	1.91	2.22	

Symmetry codes: (iii) $-x, -y, -z$; (iv) $-x, y, z$; (x) $x, -y, 1-z$; (xi) $-x, -y, 1-z$; (xiii) $x, -\frac{1}{2}-y, \frac{1}{2}+z$; (xv) $\frac{1}{2}+x, y, \frac{1}{2}-z$; (xvi) $\frac{1}{2}+x, -\frac{1}{2}+y, z$; (xvii) $\frac{1}{2}-x, -\frac{1}{2}+y, z$. † d_{min} and d_{max} are determined in the t interval where $P_{Mo(4)} \geq 0.20$.

If one considers the Eu atom as bound throughout the crystal to 12 O atoms located at the corners of a distorted EuO_{12} cuboctahedron, a wide spread is observed for the Eu—O distances (2.45–3.20 Å), which are otherwise consistent with the literature data. While smooth variations are observed for the La(1)—O distances in the modulated $LaMo_8O_{14}$ crystal, large variations [except for the Eu—O(2) bond lengths (Fig. 6)] are implied for the Eu—O distances in the Eu-containing crystals owing to the significant displacement of Eu along x. Two regions can be discerned in the crystal: in the first one, for t around 0 and 1/2, the Eu—O distances are relatively closely grouped and the Eu atom is located near the origin, which coincides roughly with the polyhedron centre; in the second region, which is rather broad and around t = 1/4, the Eu—O distances vary greatly, the Eu atom coming near some O atoms to establish strong bonds; as a result, the Eu atom is bonded to only seven O atoms and is off-centre in the polyhedron. A similar situation is observed for Nd and Sm in the two polar structures $NdMo_8O_{14}$ and $SmMo_8O_{14}$.

It should be noted that in the regions of the crystal where the Eu displacements along x are positive and the largest, the two sites Mo(4) and Mo(4^{x}) symmetry-related by 2_x are likely ($P > 0.75$) to be occupied by Mo atoms.

The ranges observed for the Mo—O distances inside the $Mo(1)O_5$, $Mo(3)O_5$ and $Mo(4)O_6$ polyhedra (Table 3) are quite consistent with the literature data, considering, for instance, the compounds $SmMo_8O_{14}$, isotypic with $LaMo_{7.7}O_{14}$ (Tortelier & Gougeon, 1997), $LaMo_8O_{14}$, a variant where *cis*-edge-sharing and *trans*-bi-face-capped Mo_8 clusters coexist in equal proportions (Kerihuel *et al.*, 1996), and $LaMo_{7.7}O_{14}$ (Leligny *et al.*, 1990).

Smooth variations of the Mo—O distances with amplitudes less than 0.02 Å are observed in the $Mo(3)O_5$ polyhedron (Table 3). The largest Mo—O distance is to O(2), the apical atom, and remains constant in all the unit cells. This property may be related to the fact that the O(2) atom is the only one which is bound to three Mo atoms throughout the crystal. Larger variations of the Mo—O distances are observed in the $Mo(1)O_5$ and $Mo(4)O_6$ polyhedra; the Mo(4)—O bonds are considered as established in the crystal zone ($-0.10 \leq t \leq 0.40$) where the occupancy probability of the Mo(4) site by Mo is larger than 0.20, an arbitrary value. These Mo—O distance variations can be explained easily from the atomic displacements; indeed, starting from the m mirror, the displacements of the Mo and O atoms increase with their average $\langle x_0 \rangle$ coordinates (see Table 2).

The V(4)—O bond lengths can be distinguished from the Mo(4)—O bond lengths since both the average positions and the displacements of the V(4) and Mo(4) sites are significantly different (see Table 2). In the crystal zones where the occupancy probability P of V is significant ($P > 0.15$), the spread of the V(4)—O distances (Table 3) appears larger (1.75–2.29 Å) than

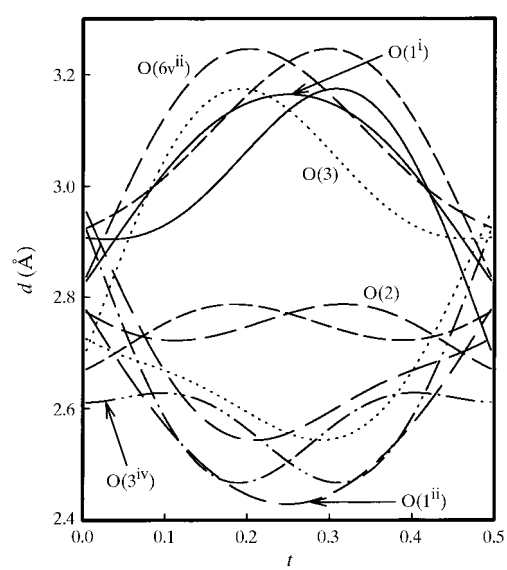

Fig. 6. The variations of the Eu—O distances as a function of t limited to the 0–0.5 interval where $P_{Eu} = 1$. Each unlabelled curve is symmetry-related to a labelled curve through a vertical line crossing the horizontal axis at t = 1/4. The two corresponding O atoms are symmetry-related in the average structure by 2_x. The uncertainties σ vary from 0.004 to 0.006 Å. Symmetry codes: (i) $-\frac{1}{2}+x, -y, -\frac{1}{2}+z$; (ii) $\frac{1}{2}-x, y, \frac{1}{2}-z$; (iv) $-x, y, z$; (vii) $-x, -\frac{1}{2}+y, \frac{1}{2}-z$.

that of the Mo(4)—O distances (1.90–2.24 Å). Otherwise, the sum of the bond valences (Brese & O'Keeffe, 1991) of the V—O bonds for V is nearly constant in these crystal zones and indicates that V in this octahedral coordination is trivalent. For the Mo atom the sum s of the bond valences (Brown & Wu, 1976) of the Mo—O bonds is nearly constant for Mo(3) ($s \simeq 3.0$) throughout the crystal, while it varies from 2.8 to 3.3 for Mo(1) and from 3.6 to 4.1 for Mo(4) in the crystal zones defined above; this variation of s for Mo(1) and Mo(4) is likely to be correlated to that of Eu in the Eu—O bonds ($2.15 < s < 2.60$). Considering the average values of s for Mo and Eu and taking into account the chemical formula, the global sum of the cationic valences is found to be roughly equal to 28.6, which is quite close to the expected value of 28 given the empirical nature of this bond-valence calculation.

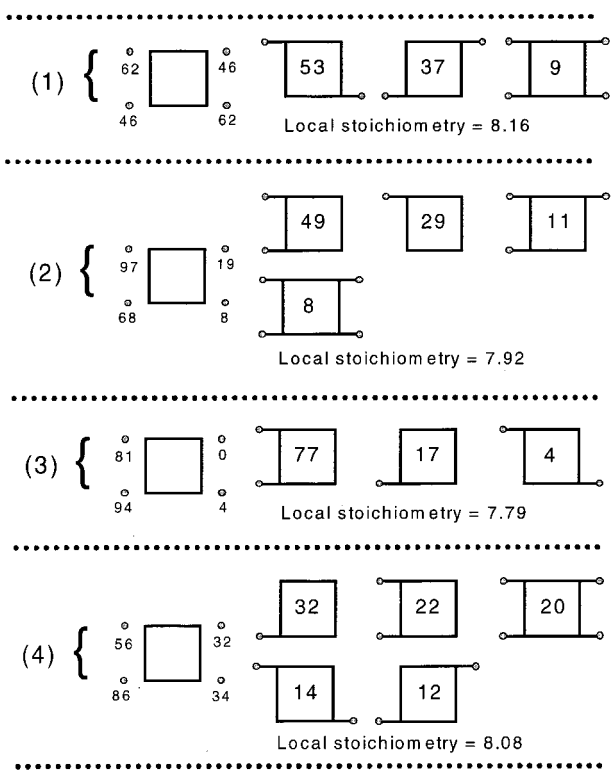

Fig. 7. The possible cluster configurations in crystal 3, which does not contain V. The numbers in parentheses specify the different environments (four in the supercell approximation) of the Mo_6 units formed by the Mo(4) sites. These environments are denoted by the same numbers in Fig. 11. For each environment the occupancy probabilities ($\times 10^2$) of the four symmetry-related Mo(4) sites are indicated with the corresponding local stoichiometry (l.s.) and the possible cluster configurations i are proposed with their p_i percentages ($\times 10^2$). The Mo_6 unit is represented by a square. If n_i is the number of Mo atoms ($n_i = 1, 2, 3$ or 4) filling the Mo(4) sites, the relations l.s. $= 6 + \sum_i n_i p_i$ and $\sum_i p_i = 1$ have to be satisfied simultaneously.

5.3. *The metallic clusters*

5.3.1. *The possible cluster configurations*. Let us discuss some results concerning the metallic clusters (MCs), considering them first as isolated blocks inside the crystal. The MC average compositions are found to be $Mo_{7.10(5)}V_{1.13(5)}$, $Mo_{7.30(1)}V_{1.10(3)}$ and $Mo_{7.96(1)}$ in crystals 1, 2 and 3, respectively. From the density modulations of Mo(4) in crystal 3, and of Mo(4) and V(4) in crystal 2 (Fig. 5), it is possible to determine the occupancy probabilities of Mo, and of Mo and V, respectively, over the four symmetry-related Mo(4) sites surrounding the Mo_6 octahedron. This calculation was performed for all the clusters along **c** in a limited number of unit cells, *i.e.* within the commensurate approximation.

In the crystal which does not contain V the MC stoichiometry varies along **c** from about 7.80 to 8.20, implying in some unit cells the existence of Mo_9 and (or) Mo_{10} clusters. The sequence observed for the Mo occupancy probabilities P inside each cluster (the upper limit for the P uncertainties is roughly 0.02) involves in most unit cells four significantly different values for P in the 0–1 interval. This result, which is implied by the density-modulation wave, can be explained by an average effect which, as specified below, originates from planar faults occurring in the (001) MC layers. To account for the different P values inside each cluster it is necessary to assume that they result from the occurrence of different cluster types which, in fact, are present in distinct zones of the crystal. Note that this occurrence of different cluster types along **c** is governed by the probability law corresponding to the density modulation; it is possible to suggest one (or several) solution for this cluster set (see Fig. 7) provided that the sum of the probabilities found for the different types of cluster is equal to one, consistent with the local stoichiometry. Thus, considering an appropriate number of P sequences running along **c**, there is evidence for several

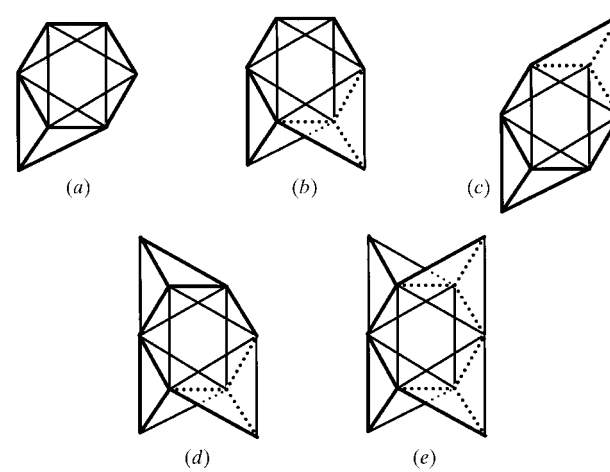

Fig. 8. The different types of cluster implied by the density modulation.

cluster types, namely Mo_7, Mo_8, Mo_9 and Mo_{10}, *i.e.* all the expected clusters (Mo_6 excepted). The Mo_7 cluster (Fig. 8*a*) has already been observed in the compounds $Sr_4Ga_3Mo_{26}O_{48}$ (Tortelier, 1997) and $RE_5Mo_{32}O_{54}$ (RE = La, Ce, Pr, Nd) (Gall *et al.*, 1993). The Mo_8 cluster, displaying the two isomeric forms *cis* (Fig. 8*b*) and *trans* (Fig. 8*c*) in about equal proportions, appears as the most likely one. These cluster types are now well known in molybdenum oxide systems. In contrast, the Mo_9 (Fig. 8*d*) and Mo_{10} (Fig. 8*e*) clusters formed by capping three or four faces of the octahedral Mo_6 unit have been observed for the first time in this system.

In crystal 2, the extreme compositions for the MC are roughly $Mo_{6.7}V_{1.6}$ and $Mo_{7.8}V_{0.6}$. Using the same method as above, it is possible to foresee the most likely cluster types involved (the upper limit for the P_V uncertainties is about 0.04). The following clusters were found: Mo_8 with mainly *cis* configurations, Mo_6V_2 with *cis* and *trans* configurations, Mo_{10}, Mo_6V, Mo_7V_3, Mo_8V_2 and Mo_6V_4; the Mo_8 and Mo_6V_2 clusters appear to be the most likely ones.

5.3.2. *Intra-cluster bonds*. The variations of the Mo—Mo distances with *t* inside the MCs are shown in Figs. 9 and 10; as these variations are quite similar for the three crystals, this discussion is limited to the second crystal (γ = 0.245). Fig. 9 shows the distances observed inside the Mo_6 units, which keep the same composition throughout this crystal, while Figs. 10(*a*) and (*b*) show the 'external' distances between Mo(4) and the Mo_6 octahedron, and V(4) and the Mo_6 octahedron, respectively. The following trends can be seen:

(i) Within the Mo_6 units, the range observed for the Mo—Mo bond lengths (2.7–2.8 Å) is quite consistent with the literature data, considering, for instance, the compounds $LaMo_{7.7}O_{14}$ (Leligny *et al.*, 1990), $SmMo_8O_{14}$ (Tortelier & Gougeon, 1997) and $LaMo_8O_{14}$, a variant containing two types of Mo_8 cluster in equal proportions (Kerihuel *et al.*, 1996).

(ii) Inside the Mo_6 unit, half the Mo—Mo distances of *f* and *g* types (Fig. 9) do not vary significantly; as a result, two parallel faces of the octahedron are not distorted under the action of the displacive modulation. Note that when one Mo(4) site is filled by Mo or V, one of the edges of this face type is shared with the tetrahedron thus formed. Otherwise, the variations of all the Mo—Mo distances show that the Mo_6 unit is a nearly regular octahedron with edges equal to 2.75 Å in the unit cells defined by the *t* values close to 0.40 and 0.90; in these crystal zones, the two Mo(4) sites symmetry-related by 2_x [Mo(4) and Mo(4^x) for t = 0.40, Mo(4^{iv}) and Mo(4^{xi}) for t = 0.90] are expected to be occupied by V atoms rather than by Mo atoms (Fig. 5). A noticeable distor-

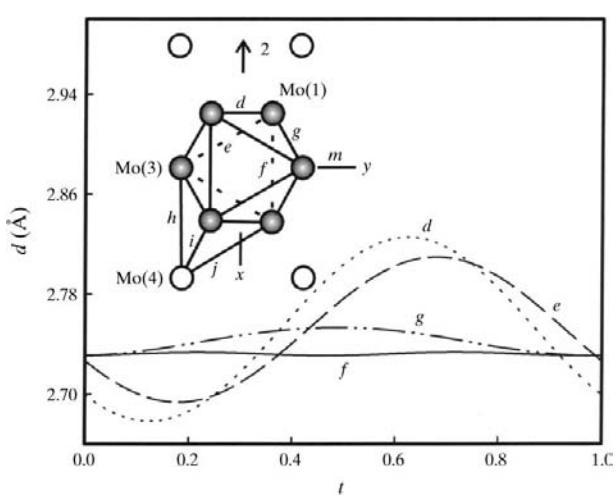

Fig. 9. The variations of the Mo—Mo distances with *t* inside the Mo_6 units; $\sigma \simeq 0.002$ Å.

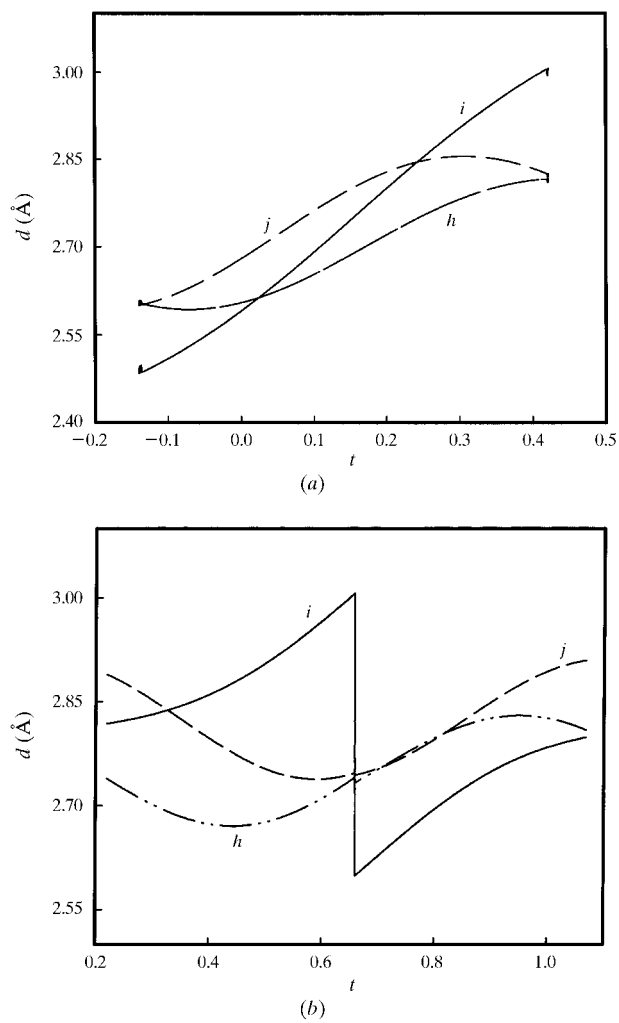

Fig. 10. The variations with *t* of the 'external' intermetallic distances; $\sigma \simeq 0.02$ Å. (*a*) Mo—Mo interactions [Mo occupies the Mo(4) site]. The labels used to define the distances are shown in Fig. 9. (*b*) V—Mo interactions [V occupies the V(4) site].

tion of the Mo_6 octahedron is present in the unit cells defined by the t values around 0.15 and 0.65 (Fig. 9) where the site pairs above are likely to be occupied by Mo ($P > 0.75$).

(iii) When the Mo(4) site is filled by Mo, three types of behaviour (Fig. 10*a*) can be seen for the 'external' Mo—Mo distances. It is possible to propose the more likely configurations for the clusters in the corresponding crystal zones by referring to literature data; for instance, in the $LaMo_8O_{14}$ variant which exhibits Mo_8 clusters with *cis* and *trans* configurations significant characteristics are observed for the corresponding Mo—Mo distances. To explain the Mo—Mo distances observed in Fig. 10(*a*), only the case of the Mo_8 cluster type (the more likely one) is considered: for $-0.14 < t < 0.02$ three strong bonds are observed with distances ranging from 2.5 to 2.7 Å. The Mo(4)—Mo(1^{xi}) distance (denoted *i* in Fig. 10*a*) is the shortest one; locally the Mo_8 clusters should have a *trans* configuration. For $0.02 \leq t \leq 0.25$ intermediate bonds are observed; the Mo(4)—Mo(3) distance (*h*) is then the shortest one, suggesting locally a *cis* configuration for the Mo_8 cluster. For $0.25 < t < 0.43$, the Mo—Mo bonds are weaker and do not seem to correspond to a standard configuration for the cluster. However, distances of the same magnitude are observed for the capping Mo atom of the Mo_7 cluster found in $Sr_4Ga_3Mo_{26}O_{48}$.

(iv) When the Mo(4) site is occupied by a V atom, a smaller range is observed for the 'external' distances (Fig. 10*b*). Two main trends are observed for the V—Mo distances; these are likely to be the *trans* and *cis* configurations of the Mo_6V_2 clusters.

5.3.3. *Inter-cluster bonds*. Owing to the displacive and the density-modulation waves, two types of cluster interactions are expected in the Eu-containing crystals. The first interaction involves two bonds denoted *l* and *n* (Fig. 2) inside the same (001) layer, while the second interaction involves a single bond denoted *m* (Fig. 11)

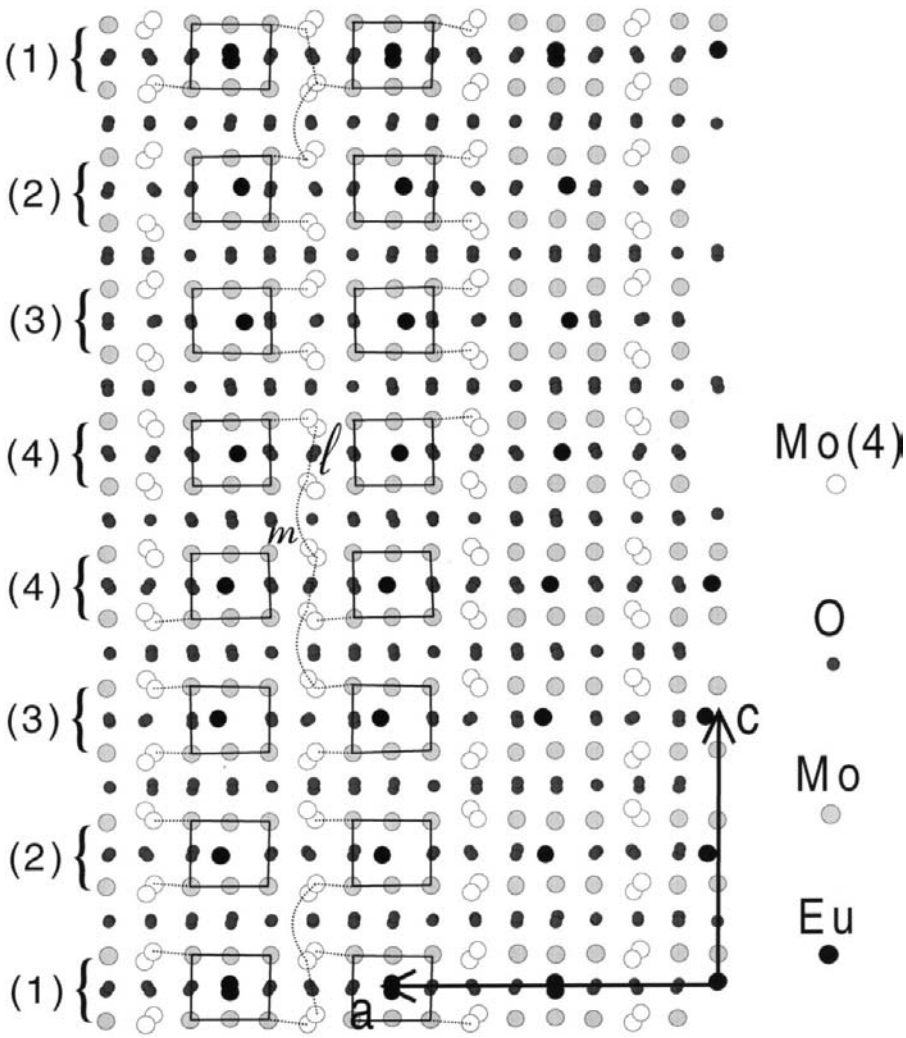

Fig. 11. A [010] projection of the modulated structure of crystal 3 in the commensurate approximation; the approximate three-dimensional symmetry is then $C2_1/c$ with 2_1 along y and the c' parameter of the supercell is equal to $7c$. The dotted curves denote the possible Mo—Mo bonds between clusters, within a particular (001) layer (*l* bonds) and between two adjacent (001) layers (*m* bonds). The numbers in parentheses (see also Fig. 7) define the different Mo environments [Mo(4) sites] of the Mo_6 octahedral units outlined with bold lines. For each environment the more likely cluster type (see also Fig. 7) is shown using dotted lines, which represent possible bonds between Mo(4) and the Mo_6 units. Note that in some parts of the crystal [environment (4)] *l* and *m* interactions are not possible for the clusters types drawn in Fig. 11 but may exist (see Fig. 7) with less likely cluster types.

between two adjacent (001) layers; these interactions are achieved *a priori via* the Mo—Mo, Mo—V or V—V pairs according to whether two neighbouring Mo(4) sites are filled by Mo, by Mo and V, or by V. The results of the average structure led to large distances for the *l* and *n* bonds (about 3.05 and 3.10 Å), and to an unrealistic distance (about 2.4 Å) for the *m* bond. Because of the rectilinear displacement along *z* of Mo (or V) on the Mo(4) site and the characteristics of the density-modulation wave, strong metallic bonds are locally implied between the clusters. This property holds for the three crystals; indeed, in some unit cells, the *l* bond distances are shorter (about 2.6 Å; Fig. 12) than the average value of 3.0 Å, while the *m* bond distances are longer (about 2.6 Å; Fig. 12) than the average value of 2.4 Å. The *n* bond type is weak in all the unit cells of the three crystals ($d \simeq 3.0$ Å). Otherwise, the probability $P' = P_iP_j$ of the existence of a pair *i*, *j* [P_i, P_j are the occupancy probabilities of the relevant Mo(4) sites by Mo or V] appears to be strongly correlated to the variations with *t* of the distances of the *l* and *m* bonds in the Mo—V (Fig. 12*a*) and V—Mo (Fig. 12*b*) interactions. The curve $P'(t)$ for the V—V pair is not plotted in Fig. 12*c* because the probabilities involved are smaller and less significant than those of the Mo—V and V—Mo pairs.

The following results can be deduced:

(i) The Mo—Mo pairs in the *l* and *m* interactions are unlikely in crystals 1 and 2 containing V ($P' < 0.07$ in all the unit cells) but may exist in some parts of the third crystal owing to the broadening along *t* of the density curve (Fig. 5). The possible Mo—Mo pairs in the *l* and *m* interactions ($d \simeq 2.6$ Å) are shown in Fig. 11, which is an [010] projection of the modulated structure in the commensurate approximation ($\gamma \simeq 2/7$).

(ii) Strong Mo—V bonds of *l* and *m* types may be implied in some unit cells of the second crystal. It is likely that they are also present in the first crystal. When Mo occupies the Mo(4) site two main situations are observed: in the first one, two strong Mo—V bonds, *l* and *m* (Fig. 12*a*), with *d* distances close to 2.6 Å may be involved simultaneously in some unit cells ($0 \le t \le 0.10$), but it is the *m* interaction which is more likely; in the second one, a single bond of *m* type (Fig. 12*a*) with $d \simeq 2.6$ Å is expected in some parts of the crystal ($0.10 \le t \le 0.20$). When V occupies the Mo(4) site, the V—Mo bond of the *m* type (Fig. 12*b*), with $d \simeq 2.6$ Å, appears more likely.

(iii) Locally, V—V interactions with distances $\simeq 2.6$ Å (Fig. 12*c*) cannot *a priori* be excluded.

5.4. *Order and disorder in the modulated crystals*

Although well resolved satellite reflections are observed, a long-range order is not perfectly established in the modulated crystals, as shown by diffuse scattering phenomena (see §3). This departure from an ideal order is also disclosed by the weakening of the intensity of the satellite reflections with respect to the intensities of the main reflections; as shown in Table 1, the scale factor K_1 ($F_o = KF_c$) in the three crystals studied is smaller than the scale factor K_0, the K_1/K_0 ratios being close to 0.6. The origin of the disorder is to be found in the filling of

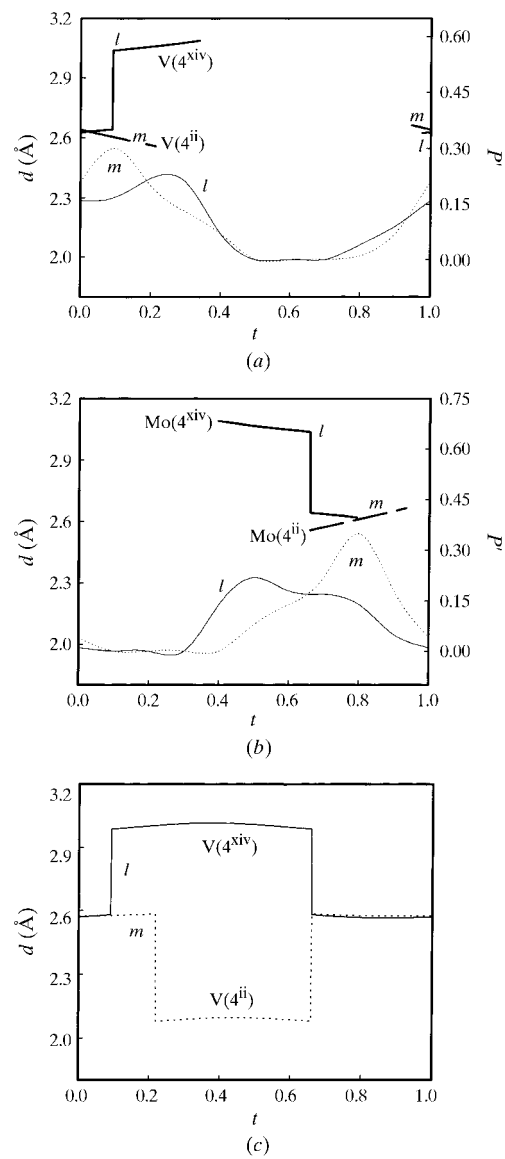

Fig. 12. The intercluster bond distances. $\sigma \simeq 0.05$ Å. (*a*) Between Mo on the Mo(4) site and V on the V(4^{xiv}) and V(4^{ii}) sites. The two curves drawn with thin lines show the variations with *t* of the probability P' ($P' = P_{Mo}P_V$) of obtaining such a Mo–V pair in the two possible *l*, *m* interactions (see text). The distance variations (bold lines) are shown in the *t* interval where $P' > 0.15$. (*b*) Between V on the V(4) site and Mo on the Mo(4^{xiv}) and Mo(4^{ii}) sites. The distance variations (bold lines) are shown in the *t* interval where $P' \ge 0.15$. (*c*) Between V on the V(4) site and V on the V(4^{xiv}) and V(4^{ii}) sites. The existence of an interaction *m* with $d \simeq 2.1$ Å is obviously impossible. Symmetry codes: (ii) $\frac{1}{2} - x, y, \frac{1}{2} - z$; (xiv) $\frac{1}{2} - x, -\frac{1}{2} - y, 1 - z$.

the Mo(4) sites surrounding the Mo_6 units by Mo or Mo and V. Indeed, density modulations $P_{Mo(4)}$ or $P_{Mo(4)}$ and $P_{V(4)}$ are implied on the Mo(4) site and the two harmonics used to describe these densities lead to intermediate values between 0 and 1 for P. This assumption of disorder is reinforced by the results of the modulations of the ADP terms. Indeed, large variations (up to 0.025 $Å^2$) about the average values are observed for U^{11} and U^{22} of Mo on the Mo(4) site, the largest values occurring in the crystal parts where $P_{Mo} \simeq 0$. In contrast, smooth variations (less than 0.005 $Å^2$) are seen for the ADP terms of Mo(1) and Mo(3) which, with the O atoms, are not affected by the disorder phenomenon. As diffuse [001]* streaks with small width along **a*** and **b*** are observed (at small θ) around some main reflections, (001) planar faults occur in some unit cells of the modulated crystals. Within a (001) layer of thickness $c/2$ a regular ordering of the metallic clusters is expected over several units along **a** or **b**. Moreover, if the C translational symmetry is locally observed in the actual crystal, then each (001) layer is built from clusters of the same type; from the results above it appears that the layers containing the Mo_8 or the Mo_6V_2 clusters in crystal 2 and the Mo_8 clusters in crystal 3 are more likely. Note that the l interaction is not possible inside a layer built from Mo_8 or Mo_6V_2 clusters in the *cis* configuration, while it may exist in some unit cells if the *trans* configuration of the Mo_8 or Mo_6V_2 clusters is achieved. Note also that it is not possible to suggest the actual sequence along **c** of the (001) cluster layers in the crystals owing to the probability law controlling the filling of the Mo(4) sites.

6. Concluding remarks

A structural model is proposed to explain the density and displacive modulations acting in $EuV_xMo_{8\pm y}O_{14}$ crystals. The three crystals studied show different compositions and different modulation periods along **c**, the direction orthogonal to the metallic cluster layers. One of the interesting results is that the amplitudes of the atomic displacements of all the atom types are quite similar in the three crystals (Table 2); considering all the unit cells, this property gives rise to a common set of interatomic distances for the crystals. In fact, it is the filling of the Mo(4) sites (by Mo, or Mo and V) surrounding the octahedral Mo_6 units which changes from one crystal to another and which likely imposes the modulation period of the crystal. Thus the sequence of the metallic cluster layers along **c** is different in the three crystals. The modulation period seems to depend mainly on the Mo stoichiometry rather than on the V stoichiometry. In fact, the third crystal, which does not contain V, is also characterized by the same type of modulation, and the V occupancy of the Mo(4) site for the other crystals seems to be rather independent of the modulation period compared with the Mo occupancy of the same site.

Let us briefly outline the main differences between the modulated structures of the Eu- and La-containing crystals.

Whereas the displacement magnitudes of the O atoms are similar in the two types of crystals, the Eu displacements are much larger than the La displacements; the displacements of the cations surrounding the Mo_6 units are also larger in the Eu-containing crystals than in the La-containing crystals. As a result, the change in the cation O-atom environments is greater in the Eu-containing crystals than in the La-containing crystals.

Different types of clusters are observed in the Eu-containing crystals: Mo_7, Mo_8, Mo_9, Mo_{10}, Mo_6V, Mo_6V_2, Mo_6V_4, Mo_7V_3 and Mo_8V_2, while only one type, Mo_8, is observed in the La-containing crystals. Otherwise, if the C translational symmetry is assumed locally in the Eu-containing crystals, then only one type of cluster with a given configuration (for instance *cis* or *trans* for the Mo_8 cluster) is observed inside a particular layer; the density modulation only acts on the stacking of the different types of layers along **c**. In contrast, in the La-containing crystals different configurations, two *cis* and two *trans*, are seen for the Mo_8 cluster inside a particular layer and it is the density modulation which is responsible for this heterogeneity inside a layer.

Finally, the fact that the Eu-containing crystals exhibit centrosymmetric structures and the La-containing crystals have polar structures also induces special features concerning mainly the stacking of the metallic clusters: strong intercluster bonds in a particular layer or between two neighbouring layers are indeed formed in some unit cells of the Eu-containing crystals, while the Mo_8 clusters are isolated blocks in the La-containing crystals.

The authors are grateful to Mrs R. Aguinet and Mrs J. Chardon for their technical assistance.

References

Boucher, F., Evain, M. & Petříček, V. (1996). *Acta Cryst.* B**52**, 100–109.
Brese, N. E. & O'Keeffe, M. (1991). *Acta Cryst.* B**47**, 192–197.
Brown, I. D. & Wu, K. K. (1976). *Acta Cryst.* B**32**, 1957–1959.
Gall, P. & Gougeon, P. (1993). *Acta Cryst.* C**49**, 659–663.
Gall, P., Toupet, L. & Gougeon, P. (1993). *Acta Cryst.* C**49**, 1580–1584.
Gougeon, P. & McCarley, R. E. (1991). *Acta Cryst.* C**47**, 241–244.
Kerihuel, G. & Gougeon, P. (1995*a*). *Acta Cryst.* C**51**, 787–790.
Kerihuel, G. & Gougeon, P. (1995*b*). *Acta Cryst.* C**51**, 1475–1478.
Kerihuel, G., Tortelier, J. & Gougeon, P. (1996). *Acta Cryst.* C**52**, 2389–2393.
Leligny, H., Labbé, Ph., Ledésert, M., Hervieu, M., Raveau, B. & McCarroll, W. H. (1993). *Acta Cryst.* B**49**, 444–454.

Leligny, H., Ledésert, M., Labbé, Ph., Raveau, B. & McCarroll, W. H. (1990). *J. Solid State Chem.* **87**, 35–43.
McCarroll, W. H., Katz, L. & Ward, R. (1957). *J. Am. Chem. Soc.* **79**, 5410–5414.
Petricek, V. & Dusek, M. (1998). *JANA*98 *Crystallographic Computing System.* Institute of Physics, Academy of Sciences of the Czech Republic, Prague, Czech Republic.
Petříček, V., van der Lee, A. & Evain, M. (1995). *Acta Cryst.* A**51**, 529–535.
Tortelier, J. (1997). Thesis, University Rennes I, France.
Tortelier, J. & Gougeon, P. (1996). *Acta Cryst.* C**52**, 1862–1867.
Tortelier, J. & Gougeon, P. (1997). *Acta Cryst.* C**53**, 668–671.
Trueblood, K. N., Bürgi, H. B., Burzlaff, H., Dunitz, J. D., Gramaccioli, C. M., Schulz, H. H., Shmueli, U. & Abrahams, S. C. (1996). *Acta Cryst.* A**52**, 770–781.
Wolff, P. M. de, Janssen, T. & Janner, A. (1981). *Acta Cryst.* A**37**, 625–636.